HST/NICMOS Imaging of Disks and Envelopes Around Very Young Stars[1]

Deborah L. Padgett[2], Wolfgang Brandner[2], Karl R. Stapelfeldt[3],
Stephen E. Strom[4], Susan Terebey[5], David Koerner[6]
[2]Caltech - JPL/IPAC, Mail Code 100-22, Pasadena, CA 91125, USA
[3]JPL, 4800 Oak Grove Drive, Mail Stop 183-900, Pasadena, CA 91109, USA
[4]NOAO, 950 N. Cherry Ave., Tucson, AZ 85726
[5]Extrasolar Research Corporation, 720 Magnolia Ave., Pasadena, CA 91106, USA
[6]University of Pennsylvania, Dept. of Physics and Astronomy, 209 South 33rd Street, Philadelphia, PA 19104-6396, USA

ABSTRACT

We present HST/NICMOS observations with $\sim 0\farcs1 \approx 15$ AU resolution of six young stellar objects in the Taurus star-formation region. The targets of our survey are three Class I IRAS sources (IRAS 04016+2610, IRAS 04248+2612, and IRAS 04302+2247) and three low-luminosity stars (DG Tau B, Haro 6-5B, and CoKu Tau/1) associated with Herbig Haro jets. The broad-band images show that the near-infrared radiation from these sources is dominated by light scattered from dusty circumstellar material distributed in a region 10 - 15 times the size of our solar system. Although the detailed morphologies of the individual objects are unique, the observed young stellar objects share common features. All of the circumstellar reflection nebulae are crossed by dark lanes from 500 - 900 AU in extent and from less than 50 to 350 AU in apparent thickness. The absorption lanes extend perpendicular to known optical and millimeter outflows in these sources. We interpret the dark lanes as optically thick circumstellar disks seen in silhouette against bright reflection nebulosity. The bipolar reflection nebulae extending perpendicular to the dust lanes appear to be produced by scattering from the upper and lower surfaces of the disks and from dusty material within or on the walls of the outflow cavities. Out of five objects in which the central source is directly detected, two are found to be subarcsecond binaries. This mini-survey is the highest resolution near-infrared study to date of circumstellar environments around solar-type stars with age ≤ 1 Myr.

Subject headings: accretion disks — circumstellar matter — stars: pre-main sequence — ISM: jets and outflows

---

[1]Based on observations with the NASA/ESA Hubble Space Telescope obtained at the Space Telescope Science Institute, which is operated by the Association of Universities for Research in Astronomy, Inc., under NASA contract NAS5-26555.

1. Introduction

Theoretical and observational investigations of star formation suggest that the formation process for low mass stars results naturally in the formation of a circumstellar disk which may then evolve into a planetary system. The current paradigm for the birth of single stars (Adams, Lada, & Shu 1987; Strom 1994, etc.) includes the following phases:

• Within a dusty molecular infall envelope, a star + nebular disk form. Most of the material destined for the star falls first onto the disk, due to the non-zero angular momentum of the infalling gas. As gas accretes onto the star, an accretion-driven stellar or disk wind develops which begins to clear envelope gas away from the rotational poles of the system. This is the "embedded young stellar object" (YSO) phase with a "Class I" spectral energy distribution (SED) characterized by a spectrum which rises beyond 2 μm because almost all the light from the star is absorbed and re-radiated by circumstellar dust at long wavelengths. In the most embedded objects, most of the scattered light may come from walls of the outflow cavity in the envelope, giving a "cometary" appearance to the circumstellar reflection nebulosity. Some extreme "Class 0" objects are completely invisible at wavelengths shorter than 25 microns and probably represent the early stages of the embedded YSO phase (André, Ward-Thompson, & Barsony 1993). This phase is thought to last for a few times 10^5 yr.

• The infalling envelope disperses, leaving an optically visible "classical" T Tauri star (CTTS) with a circumstellar disk. Accretion through the disk slows, but continues as the star gains the final few percent of its mass. This "Class II" phase lasts from 10^6 to 10^7 yr and is characterized by a spectrum which has near-to-far IR emission in excess of photospheric values, but is flat or falling longward of 2 μm. Long wavelength emission is diminished since the solid angle subtended by the disk is smaller than the envelope, intercepting and reprocessing less of the radiation from accretion processes and the stellar photosphere. As the envelope disperses, light reflected from the top and/or bottom surfaces of an optically thick disk will dominate the nebulosity, which will appear more "flattened" than for Class I sources.

• Accretion through the disk subsides due to lack of replenishment or disk gaps created by planet formation. The disk becomes optically thin, and the system evolves into a "weak-line" T Tauri star (WTTS). Its "Class III" spectrum is basically that of a stellar photosphere with a small amount of infrared excess at mid and far IR wavelengths if an optically thin protoplanetary or planetary debris disk remains. These sources would look like the optically thin disk around Beta Pictoris (Backman & Paresce 1993) if edge-on, with starlight dominating a thin, bright, elongated nebula. Unfortunately, since the IR emission from these disks are below the IRAS detection limits for nearby star-formation regions, there are currently only loose constraints on the timescale for dispersal of optically thin or "debris" disks.

This picture provides a logical context for understanding the ensemble of infrared SEDs observed for young stars (Adams, Lada, & Shu 1987), as well as the sequence of millimeter continuum brightnesses among YSOs (Saraceno et al. 1996; André, Ward-Thompson, & Barsony

1993). However, there is as yet little direct observational confirmation at spatial scales which distinguish the morphology of the circumstellar material. In particular, empirical information is lacking re: (i) large-scale geometry and distribution of material in infalling envelopes; (ii) the geometry and extent of wind-created cavities; (iii) the large-scale distribution of material within the disks. Hubble Space Telescope (HST) optical (WFPC2) and near-infrared (NICMOS) observations potentially enable us for the first time to examine the morphology of circumstellar environments during all evolutionary stages with spatial resolution of 10 - 30 AU. At this resolution, we can readily resolve and quantify structure in envelopes (expected size $\sim$ 1000 AU) and infer information on the large scale structure of disks (which are expected to have sizes spanning the range 10 to several hundred AU). Our group is carrying out a series of imaging programs aimed at quantifying the morphology of YSOs spanning the full range of evolutionary states. Our goal is to characterize the basic morphologies of objects in each SED class observable by HST, to identify common features among objects of each class, to summarize complementary ground-based data, and to identify those features which correspond to current YSO models as well as those that are not/cannot yet be predicted from such models.

Ground-based observations have revealed that many Class I young stellar objects are nebulous in the optical and near infrared. Tamura et al. (1991) found that Class I objects which excite outflows are almost always associated with compact and/or extended near-infrared nebulae. The observations of Kenyon et al. (1993) revealed that Class I YSOs in the Taurus star-formation region (distance 140 pc; Kenyon, Dobrzycka, & Hartmann 1994) often display a NIR cometary morphology which can be fit by models of a flattened envelope with a polar outflow cavity. Many of the Taurus Class I sources are also highly polarized, indicating the dominance of scattered light at short wavelengths in these systems (Whitney, Kenyon, & Gomez 1997). Lucas & Roche (1997) were able to characterize the structure of several Taurus Class I sources on subarcsecond scales and found that these sources were completely nebulous at 1 μm. A recent study by Kenyon et al. (1998) detected about half of the Taurus Class I sources in an optical spectroscopic survey using the Palomar 5-meter and the MMT, during which they determined spectral types for several of the central sources.

Previous HST observations of young stellar objects have demonstrated that high angular resolution imaging of circumstellar morphology can make significant contributions to the study of young stellar object disks and envelopes. HH 30 has been revealed to be a textbook validation of the circumstellar disk/wind paradigm (Burrows et al. 1996), with bipolar reflection nebulae separated by an optically thick flared absorption disk 450 AU in diameter and an extremely narrow jet emanating from within 30 AU of the central star. HST/WFPC2 imaging has also shown that HL Tauri, previously thought to be a directly visible classical T Tauri star, is actually an embedded system seen entirely by scattered light at optical wavelengths (Stapelfeldt et al. 1995a).

Our target sample consists of six established and probable Class I young stellar objects. The objects include three low luminosity IRAS point sources (IRAS 04016+2610, IRAS 04248+2612, IRAS 04302+2247) and three Herbig-Haro jet exciting stars (DG Tau B, Haro 6-5B, CoKu Tau/1).

The three IRAS stars are Class I infrared sources. The SED classification of the remaining sources are uncertain because they are confused with bright nearby YSOs in the large IRAS beams. These objects span a considerable range in millimeter continuum flux, which is listed in Table 1. Millimeter continuum flux is interpreted as optically thin blackbody emission from the dust around young stellar objects, and the amount of flux is related to the amount of circumstellar material (Beckwith et al. 1990; Osterloh & Beckwith 1995). The span of millimeter continuum fluxes for our sample objects corresponds to more than an order of magnitude in circumstellar masses, from about 10^{-2} $M_\odot$ for $F_{1mm} \sim 200$ mJy to $\leq 10^{-3}$ $M_\odot$ for 10 mJy (Beckwith et al. 1990). Of the six objects in our sample, four have unresolved continuum peaks at 1.3 mm as mapped by millimeter interferometry. indicating the presence of an unresolved dust disk (IRAS 04302+2247, Padgett et al. 1999; DG Tau B, Stapelfeldt et al. 1999; Haro 6-5B, Dutrey et al. 1996; IRAS 04016+2610, Hogerheijde et al. 1997). The two remaining YSOs (CoKu Tau/1, IRAS 04248+2612) have only been mapped at millimeter wavelengths with relatively large (12″) beams; however, they have the lowest circumstellar masses in any case. In order to facilitate modelling at multiple wavelengths, we chose objects for which HST/WFPC2 observations were either planned or already taken. The pre-existing WFPC2 data enabled us to select several objects with known close to edge-on "disk" orientations. As predicted by Bastien & Menard (1990) and Whitney & Hartmann (1992), and observationally demonstrated by Burrows et al. (1996), the visibility of optically thick circumstellar disks is maximized when the disk material itself occults the star, improving the contrast of the nebulosity relative to the stellar point source. The low luminosity jet source CoKu Tau/1 was chosen on the basis of its faintness at 2 microns (Stapelfeldt et al. 1997b) as well as the low radial velocity of its jet, indicating that its optical outflow is nearly in the plane of the sky (Eislöffel & Mundt 1998). Detailed comparison and multiwavelength modeling of HST/WFPC2 and HST/NICMOS images of some of these YSOs will be presented in future papers. The current paper attempts to characterize the morphology of the observed Taurus YSOs at a scale of tens of AU at wavelengths from 1.1 to 2 μm.

2. Observations and Data Analysis

2.1. HST/NICMOS observations

The observations have been obtained with HST/NICMOS (see Thompson et al. 1998 for a description of the NICMOS instrument) between August and December 1997. We used NIC2 and the filters F110W, F160W, F187W, and F205W. Exposure times in individual bands are shown in Table 2. Each target was imaged twice in each band on different portions of the NICMOS array, using the predefined spiral dither pattern. The two-step dither pattern allowed us to compensate for bad pixel/columns and the area blocked by the coronographic mask.

2.2. Re-reduction of NICMOS data

The raw data were re-reduced using the IRAF/STSDAS package CALNICA V3.1 and the latest set of reference files. Pixel masks based on the template bad pixel masks made available through STScI were created for each individual image and edited to include the actual position of the coronographic spot, transient bad pixels, and cosmic ray events which had not been detected and cleared out by CALNICA. The "photometrically challenged column #128" (Bergeron & Skinner 1997) was masked as well.

The offsets between the two subsets of each association were computed by cross-correlating the individual subsets. Using the IRAF/STSDAS package DRIZZLE (Fruchter & Hook 1997), the subsets were then re-mapped into one frame with the same pixel scale, but taking into account subpixel shifts between the individual frames, and the information in the bad pixel masks.

2.3. Deconvolution of images

The NICMOS-PSF, although well defined, has very extended wings. In order to improve the contrast of our images, we decided to deconvolve them with the aim to remove (or at least attenuate) the extended PSF features. After remapping, the images were rebinned by a factor of 2 in X and Y, and deconvolved with a synthetic point-spread function (PSF). The PSFs were computed with TINYTIM V4.4 (Krist 1997) and oversampled by a factor of 2. Because of finite sampling, deconvolution of point sources superposed on a diffuse bright background in general leads to "ringing" artifacts, unless one uses a narrower PSF (Lucy 1990, Snyder 1990). We therefore first deconvolved the TINYTIM PSF itself with Gaussian. The FWHM of the Gaussian was chosen to match the actual sampling of our data.

The deconvolution of the data was done within IDL, using an iterative Poisson maximum likelihood algorithm based on the Richardson-Lucy-scheme (Richardson 1972, Lucy 1974) and described in detail by Blecha & Richard (1989). The iteration was stopped after 5 iterations in F110W, 8-10 iterations in F160W, 10-15 iterations in F187W, and 15-20 iterations in F205W. The deconvolution reduced the flux in the extended PSF features by about a factor of 3, and gave the deconvolved images in the various filters approximately the same spatial resolution.

2.4. SYNPHOT flux calibration

In order to get an estimate on the brightness of our sources, we calculated the count rates within an aperture of 3.″8 radius (50 pixel). Sky/background values were measured on areas of the NICMOS frames which were free of diffuse emission.

Flux calibration was computed in an iterative approach, using the IRAF/STSDAS package

SYNPHOT. This step was necessary, as the photometric header keywords provided by the NICMOS calibration pipeline assume a spectral energy distribution with a constant flux per unit wavelength. The spectral energy distribution of our sources, in particular those of the three class I sources (IRAS 04016+2610, IRAS 04248+2612, and IRAS 04302+2247), deviates significantly from this assumption. Using IDL and IRAF, we first computed a model spectral energy distribution, based on the photometric header keywords. We then ran SYNPHOT for the model SED and computed a new set of photometric conversion factors. This allowed us to create a revised model SED and to derive improved photometric conversion factors. The iterative procedure was repeated until the flux values in the individual filters changed by less than 2% in consecutive iterations.

Depending on the actual shape of the spectral energy distribution, the resulting flux values in individual filters are between 25% and 180% of the initial estimates as derived from the pipeline header keywords. Aperture photometry of the sources is reported in Table 3. The quoted uncertainties are statistical errors. Systematic errors in the flux calibration (due to the unknown shape of the spectral energy distribution below 1μm and above 2μm) amount to an additional uncertainty of 10%–15%.

2.5. Photometry of Point Sources and Binaries

Magnitudes of point sources were determined using a $0\farcs5$ aperture, which excludes most of the extended, diffuse emission. The separation, position angle, and brightness ratio of the close binary sources were determined by least squares fitting based on Gaussian PSFs (see Brandner et al. 1996 for details). Point source photometry is shown in Table 4. The quoted uncertainties are statistical errors. For the binary companions deviations of the actual PSF from a Gaussian result in an additional uncertainty of $\approx$10%.

3. Results for Individual YSOs

Figure 1(a) - (f) show a three-color composite image for each of the young stellar objects in our sample. In this figure, we present "pseudo-true color" (sensitivity normalized) mappings of F110W to blue, F160W to green, and F205W to red. The scale and orientation of each image are depicted in the Figures. Figures 2(a) - (f) are the flux calibrated contour maps of each source for the F160W images. Although the images have been deconvolved and reconvolved to a common resolution, residual PSF features remain, especially in the F205W images. These artifacts appear as multicolored spots and rings surrounding the stellar PSF. We are therefore wary of interpreting structure near the Airy rings of the stars. The deconvolution has also added speckle noise to the background which has been de-emphasized in the stretches presented here.

The results are presented in order of decreasing millimeter continuum flux. To the extent that

the objects have comparable luminosities, this is equivalent to sorting from largest to smallest circumstellar masses.

3.1. DG Tau B

DG Tau B is a low-luminosity jet source located 1′ southwest of DG Tau, and its IR SED is confused with this brighter optical source. DG Tau B was first identified as a Herbig-Haro jet exciting star by Mundt & Fried (1983), and the kinematics of its optical outflow (HH 159) has been the subject of several papers (Eislöffel & Mundt 1998, Mundt, Brugel, & Bührke 1987). Radial velocities indicate that the jet is directed to within 15° of the plane of the sky. DG Tau B also drives a large molecular jet which is spatially coincident with its redshifted optical jet (Mitchell et al. 1997, 1994). The DG Tau B source has been detected in 6 cm radio continuum emission (Rodriguez et al. 1995) which is further evidence of this system's youth. Stapelfeldt et al. (1997) found that DG Tau B is resolved in HST/WFPC2 images as a compact bipolar nebula with no optically visible star.

In the HST/NICMOS composite image presented in Figure 1a, DG Tau B appears as a bipolar reflection nebula. The eastern lobe appears V-shaped, with an axis of symmetry coinciding with the direction of the blueshifted jet (Eislöffel & Mundt 1998). Therefore, we conclude that the "V" traces the walls of the blueshifted outflow cavity. At 2 μm, the stellar PSF becomes visible at the apex of the "V". Immediately to the southwest of the central source is a bright spot in the nebula along the inner edge of "V". Although this feature might be due to a companion source, the spot itself is extended relative to the PSF and, therefore, cannot be a companion seen directly. There appear to be no significant color gradients across the cavity walls. The western lobe of the nebula is several times fainter and has a much narrower opening angle. It encompasses the redshifted optical and CO jets. Several knots in the redshifted jet are visible in the 1 μm (F110W) image (Figure 3), probably due to 1.26 μm [Fe II] emission. Knots in the blueshifted jet are not obvious against the eastern lobe's bright reflection nebulosity. Separating the two lobes of bright nebulosity is a thick dust lane perpendicular to the jet which can be traced to a length of 600 AU. A dense bar of ^{13}CO(1-0) emission has recently been detected at this location by Stapelfeldt et al. (1999) using the Owens Valley Radio Observatory (OVRO) Millimeter Array.

3.2. IRAS 04016+2610

IRAS 04016+2610 is a Class I infrared source with $L_{bol} = 3.7\ L_{\odot}$ located in the L1489 dark cloud of the Taurus star-forming region (Kenyon & Hartmann 1995). Millimeter-wave observations of this source have detected an extended molecular gas core (Hogerheijde et al. 1998, Ohashi et al. 1991). This IRAS source appears as a scattered light nebula in the optical and near infrared (Lucas & Roche 1997, Whitney et al. 1997), but is centrally condensed at 2 microns. IRAS

04016+2610 powers a low velocity molecular outflow adjacent to the source (Hogerheijde et al. 1998) and has been suggested as the powering source of a more extended molecular outflow to the northwest (Moriarty-Schieven et al. 1992, Terebey et al. 1989). Several Herbig-Haro objects coincide with the lobes of these outflows (Gomez et al. 1997).

In Figure 1b, IRAS 04016+2610 appears as a unipolar reflection nebula with a point source at the apex at 1.6 μm and 2 μm. The multicolored specks around the point source are PSF artifacts which were not entirely removed by the deconvolution process. Among the sources in our NICMOS imaging sample, IRAS 04016+2610 is the brightest point source at 2 μm (Table 2), with about 75% of the flux concentrated in the PSF (Table 3). In the 1 μm image, the object is dominated by scattered light, and the highest surface brightness region is adjacent to the point source position seen at longer wavelengths. This bright patch is separated from the main part of the reflection nebula by an area of extinction extended roughly east-west. This feature is visible as a swath of reddening which cuts diagonally across the reflection nebula in Figure 1b. Between 1 μm and 1.6 μm, the shape of the reflection nebula changes significantly, from a V-shaped morphology at 1 μm to a broader bowl-shaped nebula at longer wavelengths. The symmetry axis of this nebula is well aligned with adjacent optical and blueshifted millimeter outflows (Hogerheijde et al. 1998, Gomez et al. 1997). About 3″ NNE of the point source is a faint triangular patch of reflection nebula detached from the main nebula. A dark lane oriented at PA= 80° separates this counternebula from the main nebula but does not extend to the other side of main nebula's symmetry axis. The dust lane can be traced for at least 600 AU before it loses definition in the extremely dark region to the northwest of the star. The position angle of this dark lane matches the orientation of the elongated ^{13}CO(1-0) and HCO$^+$ structures mapped by Hogerheijde et al. (1998).

3.3. IRAS 04302+2247

IRAS 04302+2247 is a Class I source with estimated L_{bol} = 0.34 $L_\odot$ (Kenyon & Hartmann 1995) located in the vicinity of the Lynds 1536b dark cloud. Undetected at 12 microns by IRAS, the infrared SED of this source peaks around 100 microns with a flux of about 10 Jy (Beichman et al. 1992). Bontemps et al. (1996) mapped a small, low-velocity CO outflow nearby which they associate with this source, and Gomez et al. (1997) have found two Herbig-Haro objects several arcminutes northwest overlying the blueshifted lobe of the outflow. IRAS 04302+2247 was studied in the near-IR at UKIRT by Lucas & Roche (1997, 1998), who published the first description of the remarkable dust lane and bipolar nebula of this system and presented near-IR polarimetry.

IRAS 04302+2247 is surely among the more spectacular young stellar objects observed by the Hubble Space Telescope. The HST/NICMOS near-IR appearance of this object in Figure 1c is dominated by the totally opaque band extending 900 AU north/south which bisects the scattered light nebulosity. No point source is detected in this source at any of the observed wavelengths. The apparent thickness of the extinction band decreases by about 30% from 1 μm to 2 μm, which accounts for the reddening seen along its edges. At 2 μm, the dust lane appears thicker at its ends

than at its center. Although this dark feature has relatively straight edges at 1 μm, at 2 μm, the lane is thicker at the ends than in the middle by a factor of two. Owens Valley Millimeter Array mapping of this source in ^{13}CO(1-0) to be presented in Padgett *et al.* (1999) indicate that the dark lane coincides with a dense rotating disk of molecular gas. The dust lane of IRAS 04302+2247 may therefore be a large optically thick circumstellar disk seen precisely edge-on.

The scattered light nebula of IRAS 04302+2247 is dramatically bipolar in morphology, with approximately equal brightness between the eastern and western lobes. The eastern lobe is only a few percent brighter than the western lobe at 1 μm and 1.6 μm, but is 15 % brighter at 2 μm. The shape of the nebular lobes is roughly similar to the wings of a butterfly, giving the object its alias "Butterfly Star in Taurus" (Lucas & Roche 1997). At 1 μm, the brightest parts of the nebula are confined to the central region along the presumed outflow axis perpendicular to the dust lane. However, the nebular morphology changes with increasing wavelength, from roughly "V"-shaped at 1 μm to more flattened along the dust lane at 2 μm. Within each lobe are a variety of bright filamentary structures subarcsecond in length and unresolved in width, some of which are curved near the dust lane. There are also areas of non-uniform extinction within the lobes which suggest a rather clumpy distribution of material. A prominent swath of extinction extends asymmetrically across the northern part of the western reflection lobe, curving smoothly into the dust lane. The central region of each lobe is fainter than the outer edges. These extinction features divide the bright lobes into quadrants, accounting for the "quadrupolar" morphology seen by Lucas & Roche (1997) and modeled as an opaque jet. One possibility is that intervening clumps of absorbing material are superposed on the symmetry axis of the reflection lobes. This interpretation would be similar to one advocated by Stapelfeldt et al. (1995a) for HL Tau. However, the darker zone does not appear to be edge-reddened as would be expected for a dark clump. Another possibility is that the darker region is an evacuated zone along the presumed outflow axis which is cleared of the reflective streamers of material seen along the cavity walls.

3.4. Haro 6-5B

Haro 6-5B, located about 20″ west of the FS Tauri T-Tauri star binary, is the source of the HH 157 optical jet. Because of its proximity to this brighter pre-main sequence system, the IRAS SED of Haro 6-5B is confused with FS Tau. This YSO was first noted as a region of compact reflection nebulosity along the emission line jet (Mundt & Fried 1983). The kinematics of the jet suggest that the outflow for this source is nearly in the plane of the sky (Eislöffel & Mundt 1998). Millimeter interferometry indicates that Haro 6-5B has compact ^{13}CO(1-0) emission (Dutrey et al. 1996). HST/WFPC2 imaging revealed that Haro 6-5B is a compact bipolar nebula bisected by a dust lane which is similar to models of a nearly edge-on optically thick disk (Krist et al. 1998). Therefore, Haro 6-5B appears very similar to the edge-on young stellar disk system HH 30 (Burrows et al. 1996).

HST/NICMOS images of Haro 6-5B generally resemble the HST/WFPC2 images of Krist et

al. (1998) with the exception that the point spread function of the star is directly detected in the near-IR images. The NICMOS color composite of Haro 6-5B is presented in Figure 1d. The source itself appears as two parallel curved reflection nebulae separated by a dark lane about 600 AU in length. The bipolar nebula is most extended along the dark lane, perpendicular to the optical outflow axis. The northeastern reflection lobe, from which the blueshifted optical jet emerges, is brighter than its southwestern counterpart at all observed wavelengths. The PSF is visible in the 1.1 μm image at the base of the northeastern lobe and contributes 60% of the light at 2 μm. Using the upper limit for stellar V magnitude from Krist et al. (1998) and assuming a late type photosphere, we determine that the lower limit of extinction toward the Haro 6-5B star is $A_V \approx 8$. If an appreciable percentage of the emission identified as photospheric is actually produced by hot dust close to the star, the extinction could be larger. About 10″ north of Haro 6-5B is a large diffuse nebula detached from the circumstellar nebulosity. This nebulosity was also detected by WFPC2 and given the designation R1 in Mundt, Ray, & Raga (1991). There is also a faint suggestion of at least one knot in the redshifted jet in the F110W and F160W images.

3.5. IRAS 04248+2612

IRAS 04248+2612 is a Taurus Class I source with a luminosity of 0.36 $L_\odot$ (Kenyon & Hartmann 1995). The object was weakly detected in HCO+ (Hogerheijde *et al.* 1997) by the James Clerk Maxwell Telescope. IRAS 04248+2612 apparently drives a small molecular outflow (Moriarty-Schieven et al. 1992) which has not been mapped. Also known as HH31 IRS, IRAS 04248+2612 is presumed to be the exciting source for HH 31 and several other small Herbig-Haro objects (Gomez et al. 1997). In the near infrared, this source has a complex bipolar reflection nebulosity which was studied with shift-and-add UKIRT infrared imaging and polarimetry by Lucas & Roche (1997). Imaging polarimetry performed by Whitney et al. (1997) led to their suggestion that this source is seen close to edge-on.

In the NICMOS images, IRAS 04248+2612 appears as a long, curving bipolar reflection nebula. The major axis of this nebula extends for at least 10″ (1400 AU) north-south, bending significantly east at the southern end and west at the northern end. The nearby string of HH objects lie along the long axis of the southern lobe close to the source, but curve eastward into an S-shaped jet at greater distances, suggesting a time-varying outflow axis (Gomez et al. 1997). The elongated reflection nebula of IRAS 04248+2612 therefore appears to define outflow channels. Although many YSO outflow cavities appear to be limb-brightened, the reflection nebula in this system is centrally brightened. Along the outflow axis within the southern lobe is an bright elongate structure which appears helical. This "corkscrew" nebulosity extends about 420 AU southwards from the central source. The northern lobe also has a bright structure which seems to be the mirror image of the southern helix. However, it appears to end or be disrupted within about 150 AU north of the central source. Although the morphology of these structures suggests an outflow origin, their similar brightness in all the wide NICMOS bands seems to indicate that

they are reflection rather than emission nebulae. An additional faint patch of reflection nebulosity is located about 750 AU to the northeast of the binary, detached from the northwest lobe of reflection nebulosity. Polarization maps presented in Lucas & Roche (1997) indicate that the position angle of the polarization vector is consistent with illumination by the distant binary.

NICMOS imaging of the IRAS 04248+2612 central source reveals that it is actually a close binary with projected separation of $\sim$ 25 AU (Table 4). Although the components of the binary are comparable in brightness, the eastern star (A) appears slightly redder than its neighbor. The presence of a close binary in this system is in accordance with its lower millimeter continuum flux relative to other Class I sources in the study. In addition, orbital motion of a binary jet source offers a plausible explanation for both the helical dusty "trail" in the southern nebular lobe and the large scale sinusoidal curving of the southern jet seen by Gomez et al. (1997). The central binary appears to peek over the north edge of a dark lane which pinches the bright nebulosity into bipolar components. This apparent dust lane is at least 450 AU in diameter and appears to extend along a position angle perpendicular to the outflow axis. The PA of the absorption lane seems to be slightly offset from the separation vector between the two stellar components.

3.6. CoKu Tau/1

CoKu Tau/1 is another faint Herbig-Haro object exciting star located in the L1495 cloud near the embedded Ae star Elias 3-1, which confuses its 60 μm and 100 μm IRAS SED. CoKu Tau/1 is detected at the shorter wavelength IRAS bands with F(12μm) = 1.18 $\pm$ 0.26 Jy and F(25μm) = 2.74 $\pm$ 0.63 Jy (Weaver & Jones 1992). Its total luminosity is estimated at only 0.065 $L_\odot$ by Strom & Strom (1994), who derived a spectral type of M2e. CoKu Tau/1 has been detected in the radio continuum at 6 cm (Skinner, Brown, & Stewart 1993), but is undetected at 1.3 mm (see Table 1). This object is the source of the small HH 156 bipolar jet (Strom et al. 1986); its kinematics suggest that the outflow is near the plane of the sky (Eislöffel & Mundt 1998).

In the HST/NICMOS near-IR images (Figure 1f), CoKu Tau/1 appears as a faint binary with four filamentary reflection nebulae curving parabolically away from the central sources. Since the optical outflow is known to emerge from between the southwestern "horns", we interpret these structures as the limb-brightened walls of outflow cavities. Within the northern cavity is a filamentary arc of material which forms a closed loop about 200 AU in size. Although the morphology of this feature is suggestive of a dark clump backlit by bright nebulosity, no enhanced reddening is seen within the loop.

Like IRAS 04248+2612, CoKu Tau/1 is a previously unrecognized binary (see Table 4). Both of these binary systems are too faint at 2 microns to have been detected by published ground-based speckle surveys (Ghez et al. 1992, Leinert et al. 1993, etc.). The CoKu Tau/1 secondary is about a magnitude fainter than the primary and is somewhat redder. The filamentary loop in the northern outflow cavity is located in the vicinity of the secondary which suggests that it is a

secondary outflow cavity.

HST/NICMOS images reveal a local minimum in surface brightness between the two cavities and along the plane of the binary stars. This feature is suggestive of a dust lane which appears much thinner than the other dust lanes seen in our survey. This might be a circumbinary ring or disk structure. The mass of the structure would have to be small, since the millimeter continuum limits the mass to less than 10^{-3} $M_{\odot}$. However, very little dust mass is required to produce a disk which is optically thick at near-infrared wavelengths, and, therefore, visible as a dust lane when at near edge-on inclinations.

4. Discussion

4.1. Dust Lane Properties

All of the young stellar objects imaged in the current NICMOS survey have a morphology which includes a dark lane crossing the scattered light nebula. Table 5 lists morphological parameters for the dust lanes seen in the NICMOS images of young stellar objects. The lengths and thicknesses of dust lanes were determined by making cuts across the feature midplane perpendicular to the major axis. The minor axis was measured by averaging 5 cuts through the center of the dark lane. In cases where the center of the dust lane is adjacent to a PSF, we determined the dust lane thickness by taking the mean of cuts on both sides of the PSF, beyond the Airy ring and other PSF artifacts. The dip in the brightness profile caused by the dust lane was fit by a Gaussian using the IRAF tool IMPLOT, and the derived full width half maximum of this feature is the "apparent thickness" or minor axis given in the results section and Table 5. The major axes of the dark lanes were determined by noting the radial distance from the photocenter at which the dip in the surface brightness profile was less than 10% of its maximum depth or where the feature widened to twice the FWHM at or near the photocenter. Although some of these features can be traced to greater distances, our intent was to place a lower limit on the disk extent without confusing it with the separation of cavity walls. Better quantification of disk parameters awaits the application of multiple scattering models in future papers. "PSF visibility" gives the filter at which a stellar PSF was detected, and the "+" indicates that the PSF was detected at all longer wavelengths.

The lengths of these dust lanes vary within our sample from 500 AU to 1000 AU. The apparent thicknesses of these dark features range from 50 AU - 340 AU. These widths do not represent the actual scale height of dense material, but rather define surfaces where optical depth ≈ 1 at NIR wavelengths for dusty circumstellar structures. The apparent thicknesses of the dust lanes seem to be related to the amount of millimeter continuum, in that objects with more 1 mm emission have thicker lanes. In addition, comparison of the dust lane position angles (Table 5) with the position angles of known outflows (Table 1) reveals that the lanes are perpendicular to outflows in almost every case. Finally, in the dust lanes of IRAS 04016+2610, Haro 6-5B, and

IRAS 04302+2247, are spatially coincident with dense, possibly rotating, molecular bars mapped by millimeter interferometry (Hogerheijde et al. 1998, Dutrey et al. 1997, Padgett et al. 1999, Stapelfeldt et al. 1999).

Based on these lines of evidence, we conclude that the absorption bands seen in the HST/NICMOS images are probably optically thick circumstellar disks seen in silhouette against reflection nebulosity. The same interpretation has been offered for dark elongated features seen in HST imaging of several other YSOs including HH 30 (Burrows et al. 1996) Orion 114-426 (McCaughrean et al. 1998), Haro 6-5B (Krist et al. 1998), and HK Tau/c (Stapelfeldt et al. 1998). As explained in considerable detail by these authors, optically thick disks are completely opaque at optical and NIR wavelengths, with hundreds to thousands of magnitudes of extinction on a line of sight through the midplane. Therefore, the disks themselves are dark, while their upper and lower surfaces are illuminated by the central source. Models for disks of this sort are presented in Bastien & Menard (1990), Whitney & Hartmann (1992, 1993), Fischer, Henning, & Yorke (1996), Burrows et al. (1996), and Wood et al. (1998). Flattened envelopes may also produce dust lanes, as the models of Whitney & Hartmann (1993) indicate; kinematics from millimeter interferometry are required to differentiate these components of circumstellar material.

Scattered light models of optically thick circumstellar disks and flattened envelopes predict that the appearance of a YSO will vary according to disk mass and inclination relative to the line of sight. Optically thick circumstellar disks viewed within a few degrees of edge-on will entirely occult the star due to high extinction in the midplane. Conversely, if they are viewed pole-on, the dynamic range required to detect light reflected from the disk is predicted by theory to be beyond the capability of early 1990's technology (Whitney et al. 1992). Edge-on disk systems are detected only in scattered light even at mid-IR wavelengths (Sonnhalter et al. 1995). There are currently three known edge-on disk sources: HH 30, Orion 114-426, and HK Tau/c, to which the current study can add a fourth - IRAS 04302+2247. Edge-on disks appear as concave nebulae of similar brightness which are separated by a flared dark lane. The apparent thickness of the lane increases with disk mass, ranging from $0\farcs1$ (at the distance of Taurus) for 10^{-4} $M_\odot$ to ten times that for 10^{-2} $M_\odot$ (Burrows et al. 1996). In addition, the apparent thickness of the disk will also vary with wavelength, becoming thinner at longer wavelengths. In systems which are slightly more than 10° from edge-on, the flared outer parts of the disk or the optically thick base of the envelope may occult the star at short wavelengths, but a PSF may be visible at longer wavelengths. In addition, one nebula will be considerably brighter than the other. In the current sample, DG Tau B fulfills these criteria, since the PSF is effectively undetected at 1 μm. We also note that no PSF was detected for Haro 6-5B in WFPC2 8000Å images (Krist et al. 1998); however, the stellar PSF was detected for this source in all of our NIR bands. Unlike envelope sources, Class II T Tauri stars have no circumstellar material except in the disk plane; therefore, they rarely have the gradation of extinction seen in embedded YSOs (invisible at V, bright at K). Depending on their disk inclination, T Tauri stars will either be bright with little circumstellar extinction or nebulosity, or they will be almost invisible at optical and NIR wavelengths (Stapelfeldt et al. 1997).

Although the distribution of circumstellar material in YSOs is unquestionably flattened, the kinematics of this material is still controversial. Models which postulate a flattened, infalling envelope surrounding a small, geometrically flat rotating disk are quite successful in explaining the scattered light distribution around YSOs (Whitney & Hartmann 1992, 1993; Hartmann et al. 1994). Lucas & Roche (1997) simulated the scattered light distribution in their ground-based images of IRAS 04302+2247 with a model incorporating an Ulrich envelope. However, such models are less successful in reproducing the scattered light distribution from HH 30. In this case, the circumstellar nebulosity is better modeled as a large optically-thick edge-on circumstellar disk (Wood et al. 1998). Recent high-resolution molecular line observations are beginning to clarify the kinematic nature of the material in these large "disks". Rotating CO structures around many YSOs with sizes from 100 AU - 1600 AU have been mapped using millimeter interferometers (Koerner & Sargent 1995, Dutrey et al. 1996, Hogerheidje et al. 1998). The disk around the T Tauri star GM Aurigae, which has been detected in reflected light by HST (Stapelfeldt et al. 1995b), shows a Keplerian rotation curve out to a radius of 500 AU (Dutrey et al. 1998). Those YSOs in the current survey which have been imaged via millimeter interferometry (IRAS 04016+2610, Hogerheijde et al. 1998; Haro 6-5B, Dutrey et al. 1996; DG Tau B, Stapelfeldt et al. 1999; IRAS 04302+2247, Padgett et al. 1999) all show concentrations of dense molecular gas close to the star. Unfortunately, the $\sim 3\farcs0$ resolution at which these YSOs have been mapped in the millimeter allows only a rough correspondence with features seen in HST images. OVRO Millimeter Array observation of IRAS 04302+2247 by Padgett et al. (1999) have confirmed that the dense material along the dust lane in this source also appears to be rotating. These observations suggest that the dense material within the YSO dark lanes seen by HST is rotating, and, possibly, centrifugally bound.

4.2. Properties of Bipolar Nebulosity

In most of the YSOs in the current sample, the symmetry axis of the bright reflection nebulae (perpendicular to the dust lanes) correspond well to the outflow position angles determined by previous studies. Table 1 lists outflow position angles, and Table 6 contains the position angle of the nebula symmetry axis (θ_{sa}). The "major axis" in Table 6 is the extent of the nebula along the symmetry axis, and the "minor axis" is the extent perpendicular to the symmetry axis. Only IRAS 04302+2247 is linked to a jet which has a very different position angle from the reflection nebula symmetry axis. HH 394 lies several arcminutes to the northwest of IRAS 04302+2247, forming a loose chain of HH objects which point back in the direction of the IRAS source (Gomez et al. 1997). The HH objects coincide well with the position of a blue-shifted clump of ^{12}CO(1-0) which was presumed to be part of the IRAS 04302+2247 molecular outflow by Bontemps et al. (1996). However, this optical and molecular outflow has a position angle which is only 20° offset from the dust lane ("disk" plane)! One possible explanation is that the disk is not perpendicular to the outflow for this source. However, we prefer to conclude that these optical and molecular outflows are probably unrelated to IRAS 04302+2247 and are instead part of an outflow from

another, more distant source, as seen frequently in Orion (Reipurth et al. 1997) and the Perseus Molecular Cloud (Bally et al. 1997). A similar situation may exist for the extensive molecular outflow located to the northwest of IRAS 04016+2610 (Terebey et al. 1989).

The reflection nebulosity associated with the current sample of young stellar objects is most often bipolar, although the detailed structure of each nebula is unique. Since the axis of known outflows tends to coincide with the symmetry axis of the reflection nebulae and the lobes are often extended along the outflow directions, it appears that the bright nebulosity most often traces the $\tau = 1$ scattering surface of dusty material in outflow cavities. Outflow cavities are presumed to represent the polar regions of circumstellar disk/envelope systems which have been cleared of dense gas by stellar jets (e.g. Raga 1995) or wide-angle outflows (e.g. Li & Shu 1996). Larger scale versions of these structures have long been known from ground-based NIR imaging (Terebey et al. 1991, Kenyon et al. 1993, Lucas & Roche 1997) and molecular line observations with millimeter interferometry (Bontemps et al. 1996, Hogerheidje et al. 1998). Hogerheidje (1998) describes the walls of outflow cavities as regions where outflowing gas interacts with infalling material in the envelope. Outflow cavities are commonly limb-brightened, especially at millimeter wavelengths (e.g. Bontemps et al. 1996), as seen for DG Tau B and CoKu Tau/1 in the current sample, and may be either conical (V-shaped) or paraboloidal in shape. The object with the smallest clearly defined opening angle for its V-shaped cavity is DG Tau B which also has the largest mass of circumstellar material. The single star with the lowest circumstellar mass (Haro 6-5B) also has the largest opening angle. The two single sources with intermediate circumstellar masses (IRAS 04016+2610, IRAS 04302+2247) also have morphologies in between these extremes, with conical nebulae at short wavelengths and more flattened morphologies at 2 μm. This suggests an evolutionary effect by which the cavity walls are widened as the circumstellar mass decreases.

The bipolar nebula of Haro 6-5B is unlike the other objects in that the scattered light is extended parallel, rather than perpendicular, to the dust lane bisecting the nebula. In this case, the scattered light appears qualitatively similar to models of edge-on disks used to fit the optical scattered light distribution of HH 30 (Burrows et al. 1996) and HK Tau/c (Stapelfeldt et al. 1998); however, the inclination is far enough from edge-on ($\sim 10°$; Krist et al. 1998) to permit the star to be directly detected in the NIR. Thus, it appears that the local circumstellar nebulosity of Haro 6-5B probably traces the upper and lower surfaces of a flared, optically thick circumstellar disk. Like HH 30, Haro 6-5B seems to have reached a stage where the scattered light distribution is dominated by the disk rather than the envelope, but sufficient material remains in the accretion disk to drive an energetic stellar jet.

Many YSO outflow "cavities" are not completely evacuated of dusty material. Every object (except possibly Haro 6-5B) that we observe in our HST/NICMOS survey has structures within the presumed outflow zone which are physically thin but are tens to hundreds of AU in length. In the case of IRAS 04302+2247, the limb brightened cavity walls encompass a plethora of these filaments. The most spectacular case of a filled outflow cavity is IRAS 04248+2612 where the polar regions are centrally brightened by an apparent dusty helical outflow channel. Many of

these bright filaments features are arcuate, and some form loops elongated in the outflow direction as in the case of CoKu Tau/1. Similar features have been identified in the HST/NICMOS YSO observations of Terebey et al. (1999), as well as the ground-based imaging polarimetric studies of Lucas & Roche (1997) and Whitney et al. (1997). The kinematics of these high-surface brightness arcs are unknown; however, it is plausible that they are related to infalling or outflowing material in the envelope. Repeated observation of such features with HST/NICMOS might reveal the dynamics of small scale structures within the cavities of YSOs.

4.3. Effect of Binarity on Circumstellar Morphology

In the course of our survey, we found two previously unknown binaries with projected separations of $\sim$ 30 AU. These two sources have the lowest millimeter continuum fluxes of the YSOs in our sample (cf. Table 1). This is consistent with the results of Osterloh & Beckwith (1995) who found that millimeter continuum flux was diminished among known binaries with a separation of less than 100 AU. In both cases, we have evidence to suggest a circumbinary disk in the form of apparent dust lanes relatively well-aligned with the separation vector of the stellar components. For CoKu Tau/1 the possible dust lane is very thin and is only distinguished with difficulty between the curving arcs of the outflow cavity walls.

In young close binary systems, theory suggests that the orbital motion of the stellar components should clear a central hole in any circumbinary disk. Depending on the eccentricity of the binary orbits, the inner edge of the circumbinary disk is predicted to be at a distance of 2 - 3 times the semi-major axis (Artymowicz & Lubow 1994). Evidence for central holes in the CoKu Tau/1 and IRAS 04248+2612 systems is lacking for the NICMOS data, since the objects were selected to be nearly edge-on, and the stellar PSFs make direct detection of the gap impossible. However, the existence of central holes in these systems are plausible, given the evidence from other young binaries. Among young stars, the GG Tau circumbinary ring is a spectacular face-on example of a disk with a cleared central region (Roddier et al. 1996, Koerner, Sargent, & Beckwith 1993). Despite the central hole, the GG Tau binary components show ample spectroscopic evidence of accretion, indicating that material is bridging the gap and falling onto the stars. The active Herbig-Haro jets emanating from both IRAS 04248+2612 and CoKu Tau/1 indicate that accretion is continuing in these systems as well.

Evidence is mounting that disks around individual stars clear from the inside out, possibly as a result of planet formation processes. It has long been known that the central 100 AU of the Beta Pictoris debris disk is depleted of dusty material and this appears to be true for other debris disks as well (Backman & Paresce 1993). Recently, mid-infrared imaging of HR 4796A (Koerner et al. 1998, Jayawardhana et al. 1998) and submillimeter maps of Epsilon Eridani (Greaves et al. 1998) have shown that inner disk holes in the absence of close binary companions may be common in younger disks and disks around solar-type stars. These stars range in age from about 20 Myr (HR 4796A) to $\sim$ several hundred million years in age (Epsilon Eridani, Beta Pictoris,

etc.). However, this disk clearing may occur at a far younger age for close binaries, dispersing the material required to make planets in the inner $\sim$ 100 AU region while retaining a ring of dusty gas in the outer parts of the circumbinary disk.

Despite the apparently diminished disk masses in the two binary systems, their large scale morphology suggests that both objects are very young. In CoKu Tau/1, nebulosity stretches for many hundreds of AU from the central sources, indicating the presence of extended circumstellar material in this system. The bipolar nebula of IRAS 04248+2612 is very elongated in the outflow direction, appearing as a relatively narrow channel in the surrounding cloud medium. Both YSOs are in extremely opaque parts of their respective clouds, without obvious neighbors or background stars. If these two objects are indeed very young ($\leq$ 1 Myr) sources, they provide further evidence that disk evolution may be accelerated in close binaries. (Osterloh & Beckwith 1995, Jensen & Mathieu 1997, Meyer et al. 1997).

It is interesting that the dust lane in IRAS 04248+2612 is not aligned with the separation vector between the stellar components. There are at least two possible explanations. The most tantalizing is that the disk is inclined relative to the orbit plane of the binary. Papaloizou & Terquem (1995) have theoretically modeled the tidal perturbations of YSO disks by companions on inclined circular orbits and have suggested that observable warps in the disk are a likely outcome. This interpretation has been applied to the warp in the Beta Pictoris disk, where an unseen planetary mass companion is presumed to excite the disk plane asymmetries (Mouillet et al. 1997). A more prosaic and likely explanation notes that because the disk is not precisely edge-on, the projected binary component separation vector need not be in the plane of the disk. From our vantage point, the orbit of the secondary would describe a long and narrow ellipse with minor axis angular size equivalent to the tilt of the orbital plane from an edge-on configuration. Another consequence of this configuration is that the projected separation of the binary components may be much smaller than their physical separation.

4.4. A Morphological Sequence of Pre-Main Sequence Circumstellar Material?

Combining the current NICMOS sample of YSOs with high resolution observations of young circumstellar disks in the literature, we can begin to relate high resolution scattered-light morphologies to evolutionary status of circumstellar material around solar-type young stars. Our goal is to estimate relative placement of the objects in our small sample in the context of pre-existing evolutionary scenarios. Presuming that millimeter continuum observations are a reasonable measure of circumstellar masses, we would order the present objects in the following sequence from most massive to least massive: DG Tau B ($\sim$ 320 mJy), IRAS 04016+2610 (180 mJy), IRAS 04302+2247 (149 mJy), Haro 6-5b (134 mJy), IRAS 04248+2612 (99 mJy), and CoKu Tau/1 ($\leq$ 12 mJy). In the objects with greater millimeter continuum flux such as DG Tau B and IRAS 04016+2610, the NICMOS images indicate a large amount of material above the midplane in the form of outflow cavity walls which are optically thick at visual wavelengths, but

become largely transparent at 2 μm. It is these circumstellar structures, which can be understood as the interaction zone between the infalling circumstellar envelope and the polar outflows, which cause many Class I sources to be very faint in the optical, yet bright at 2 μm. The extinction in the cavity walls is extremely non-uniform, as evidenced by the curving swaths of reddening seen above the "disk" plane in IRAS 04016+2610 and IRAS 04302+2247. These streamlined structures could be related to infall as discussed in Terebey et al. (1999). According to the current paradigm of star formation, sources with an extensive envelope should be the youngest objects, and we identify DG Tau B and IRAS 04016+2610 as good examples of envelope dominated systems. The importance of the envelope component in the IRAS 04016+2610 system has been highlighted by Hogerheijde et al. (1997), who found that half or more of the circumstellar mass indicated by millimeter continuum may originate in a resolved envelope. Envelope systems have been often been called "optically invisible protostars" since the extinction in the material above the midplane guarantees that the source appears very red even at moderate inclinations.

Among our sample, IRAS 04302+2247 may be at an intermediate stage between envelope dominated and disk dominated systems. Although the NICMOS images show evidence of material above the disk plane, the dense matter appears to be confined to near the disk plane. The decreasing apparent thickness of its dust lane with increasing wavelength clearly indicates a vertical density gradient. The faintness of this object at all wavelengths is a function of inclination rather than youth; it is seen almost precisely edge-on. YSOs such as IRAS 04302+2247 are plausibly in a "big disk/dispersing envelope" stage. Probably most of the more active T Tauri stars with healthy millimeter continuum emission are in a similar stage. A good example of a similar object seen at a less favorable inclination is GM Aurigae (Stapelfeldt et al. 1995b). The disk extends far enough from the central stars in this system to be visible as compact circumstellar nebulosity even at optical wavelengths. Further analysis of recent millimeter interferometry for IRAS 04302+2247 should indicate the relative percentage of mass in the disk versus the envelope, clarifying the evolutionary state of this object (Padgett et al. 1999).

The next stage of evolution appears to be represented by objects such as HH 30 and possibly Haro 6-5B, where the scattered light nebulosity adjacent to the star appears to originate entirely from the surface of the optically thick disk. The difference between Haro 6-5B and its analogue HH 30 appears to be entirely due to variations in disk mass. It seems plausible that once the envelope has dispersed, the disk begins to diminish in mass due to accretion onto the star and planetary system, as well as associated outflow events. By the time that jet emission has ceased, edge-on disks will become difficult to see due to the thinness of the dust lane (Stapelfeldt et al. 1998). We have yet to see an optically thin disk in optical or NIR wavelengths around a certifiable solar-type pre-main sequence star since the IRAS survey was not sensitive enough to detect optically thin disks at the distance of nearby star-forming regions. We await WIRE and SIRTF to identify these potentially very interesting targets for high resolution imaging.

The very lowest circumstellar masses seen for pre-main sequence stars are in binary systems such as IRAS 04248+2612, CoKu Tau/1 and HK Tau/c (Stapelfeldt et al. 1998), where the effects

of the companion have likely been to clear a hole in a circumbinary disk or tidally truncate the circumsecondary disk. If close binary systems indeed experience substantially accelerated disk evolution as suggested by the current study, then this sizable percentage of YSOs will defy the morphological sequence for single stars, since their disks may dissipate prior to envelope clearing. Again, high resolution millimeter observations may clarify the evolutionary status of these objects.

4.5. Detailed Morphology Versus IR SED

In the past decade, our progress in understanding star and planet formation has largely depended on interpretation of young star SEDs from the near-IR to millimeter wavelengths. The mid-to-far IR excesses measured by IRAS allow us to infer the existence of circumstellar disks and envelopes around young stellar objects and estimate their frequency and timescale for dissolution (Strom et al. 1989). The availability of 15 AU resolution observations of circumstellar structures provides a testing ground for models based on SEDs. For example, in the current study IRAS 04248+2612 and IRAS 04302+2247 have very similar spectral energy distributions (Figure 4), especially in the wavelength range covered by the IRAS satellite. However, comparison of the HST/NICMOS images for these objects demonstrate that the detailed morphology of these sources is quite distinct from each other, as discussed in Sections 3.2 and 3.3. In particular, the IRAS fluxes do not provide any indication of binarity for IRAS 04248+2612. Since the IRAS bands are sensitive to circumstellar material at $\leq$ 1 AU - 100 AU, it would seem that small circumstellar disks are probably still present in the close binary system. The only hint of binarity found in the SED is the lower 1 mm continuum flux for IRAS 04248+2612 (Osterloh & Beckwith 1995). The inclination of IRAS 04302+2247 is suggested by its IRAS non-detection at 12 microns. Radiation transfer models of edge-on disks suggest that they are viewed primarily in scattered light, and are thus exceptionally faint, out to wavelengths exceeding 25 μm (Sonnhalter et al. 1995). ISO observations of the edge-on disk system HH 30 appear to confirm these predictions for that object (Stapelfeldt & Moneti 1998). The significance of factors such as source multiplicity, disk extent, orientation, and gaps, dynamical structures in the polar outflow zones, and interstellar environment can only be determined by imaging at scales of smaller than tens of AU. Modelling of high-resolution optical and NIR images complements information derived from SED modelling in providing an accurate depiction of the circumstellar environment of YSOs. The extremely high sensitivity and improved resolution of upcoming mid-to-far IR space telescopes such as WIRE and SIRTF will extend the IRAS results to more evolved systems and identify potential new targets for high-resolution imaging.

5. Conclusions

We observed six young stellar objects at 1.1 μm - 2 μm with HST/NICMOS. Images with 15 AU resolution were successfully obtained for young stellar objects systems spanning a

range of circumstellar masses as derived from millimeter continuum emission. The near-infrared morphology reveal conical to parabolic bipolar reflection nebulae crossed by dark lanes. We identify the dark lanes as circumstellar disks of dimension 500 AU - 1000 AU seen at near edge-on inclinations. Millimeter interferometry available for some of the sources provides evidence of rotational motion for material in these disks. We identify the bipolar reflection nebulae as infalling envelopes illuminated by the central stars, and, in some cases, the top and bottom surfaces of optically thick circumstellar disks. The limb-brightened cavities noted in several sources most likely represents the boundary between the infalling envelope and accretion-driven outflow. If so, the opening angles of the cavities are in contrast to the narrowly collimated jets observed within the cavities for some sources. Evolutionary effects are suggested by the increase in cavity opening angle as disk mass (traced by millimeter continuum emission) decreases. In addition, although two sources found in our study to be close binaries have the smallest disk masses, their extended morphology and IRAS SEDs closely resembles other envelope-dominated YSOs. This suggests accelerated disk evolution for close binary stars.

The authors acknowledge contributions by S. Kenyon, as well as helpful comments by an anonymous referee. Deborah Padgett and Wolfgang Brandner gratefully acknowledge support from the NASA/WIRE project and STScI, as well as the tireless efforts of the NICMOS instrument team in making these observations possible. Support for this work was provided by NASA through grant number STScI GO-7418.01-96A from the Space Telescope Science Institute, which is operated by the Association of Universities for Research in Astronomy, Incorporated, under NASA contract NAS5-26555

REFERENCES

André, P., Ward-Thompson, D., Barsony, M. 1993, ApJ 406, 122

Adams, F. C., Lada, C. J., Shu, F. H. 1987, ApJ 312, 788

Artymowicz, P., Lubow, S. H. 1994, ApJ 421, 651

Backman, D. E., Paresce, F. 1993, in *Protostars and Planets III*, (University of Arizona:Tucson), ed. E. Levy & J. Lunine, pp. 1253-1304

Bally, J., Devine, D., Alten, V., Sutherland, R. S. 1997, ApJ 478, 603

Bastien, P., Menard, F. 1990, ApJ 364, 232:

Beckwith, S. V. W., Sargent, A. I., Chini, R. S., Guesten, R. 1990, AJ 99, 924

Beichman, C.A., Boulanger, F., & Moshir, M. 1992, ApJ 386, 248

Bergeron, L.E., Skinner, C.J. 1997, AAS 191, 1004

Blecha, A., Richard, L. 1989, in 1st ESO-ST-ECF Data Analysis Workshop, p. 209

Bontemps, S., André, P., Terebey, S., & Cabrit, S. 1996, A&A 311 858

Brandner, W., Alcalá, J. M., Kunkel, M. et al. 1996, A&A 307, 121

Burrows, C. J., Stapelfeldt, K. R., Watson, A. M. et al. 1996, ApJ 473, 437

Dutrey, A., Guilloteau, S., Duvert, G. et al. 1996, A&A 309, 493

Dutrey, A., Guilloteau, S., Prato, L., Simon, M., Duvert, G., Schuster, K., Menard, F. 1998, A&A 338, L63

Eislöffel, J., Mundt, R. 1998, AJ 115, 1554

Fischer, O., Henning, T., Yorke, H.W. 1996, A&A 308, 863

Fruchter, A.S., Hook, R.N. 1997, in Applications of Digital Image Processing XX, Proc SPIE, Vol. 3164, ed. A. Tescher, in press.

Ghez, A. M., Neugebauer, G., Matthews, K. 1993, AJ 106, 2005

Gomez, M., Whitney, B.A., and Kenyon, S.J. 1997, AJ 114, 1138

Greaves, J. S., Holland, W. S., Moriarty-Schieven, Jenness, T., Dent, W. R. F., et al. 1998, ApJL in press

Hartmann, L., Boss, A., Calvet, N., Whitney, B. 1994, ApJ 430, 49

Hogerheijde, M.R., van Dishoeck, E.F., Blake, G.A., van Langevelde, H. 1997, ApJ 489, 293

Hogerheijde, M. R., van Dishoek, E. F., Blake, G. A., van Langevelde, H. J. 1998, ApJ 502, 315

Jayawardhana, R., Fisher, S., Hartmann, L., Telesco, C., Pina, R., Fazio, G. 1998, ApJL 503, L79

Jensen, E.L.N., Mathieu, R.D. 1997, AJ 114, 301

Kenyon, S. J., Whitney, B. A., Gomez, M., Hartmann, L. 1993, ApJ 414, 773

Kenyon, S. J., Dobrzycka, D., & Hartmann, L. 1994, AJ 108, 1872

Kenyon, S.J., Hartmann, L. 1995, ApJS 101, 117

Kenyon, S. J., Brown, D. I., Tout, C. A., Berlind, P. 1998, AJ 115, 2491

Koerner, D. W., Sargent, A. I., Beckwith, S. V. W. 1993, ApJ 408, 93

Koerner, D. W., Sargent, A. I. 1995 AJ 109 2138

Koerner, D. W., Ressler, M. E., Werner, M. W., Backman, D. E. 1998, ApJ 503, 83

Krist, J. 1997, The TinyTim User's Guide V4.4

Krist, J., Stapelfeldt, K. et al. 1998, ApJ 501 841

Leinert, Ch., Zinnecker, H., Weitzel, N., Christou, J., Ridgway, S.T., Jameson, R., Haas, M., and Lenzen R., 1993, A&A 278, 129

Li, Z. Y., Shu, F. H. 1996, ApJ 472, 211

Lucas, P.W., Roche, P.F. 1997, MNRAS 286, 895

Lucas, P.W., Roche, P.F. 1998, MNRAS, in press

Lucy, L.B. 1974, AJ, 79, 745

Lucy, L.B. 1990, in *The Restoration of HST Images and Spectra*, eds. R.L. White & R.J. Allen, p. 80

McCaughrean, M.J., Chen, H., Bally, J., Erickson, E., Thompson, R., Rieke, M., Schneider, G., Stolovy, S., and Young, E. 1998 ApJ 492, 157

Mitchell, G.F., Hasegawa, T.I., Dent, W.R.F., Matthews, H.E. 1994, ApJ 436, 177

Mitchell, G.F., Sargent, A.I., Mannings, V. 1997, ApJ 483, 127

Mouillet, D., Larwood, J. D., Papaloizou, J. C. B., Lagrange, A. M. 1997, MNRAS 292, 896

Moriarty-Schieven, G.H., Wannier, P.G., Tamura, M., Keene, J. 1992, ApJ 400, 260

Moriarty-Schieven, G.H., Butner, H.M., Wannier, P.G. 1995, ApJ 445, 55

Mundt, R., and Fried, J. W. 1983 ApJ 274 L83

Mundt, R., Brugel, E. W., and Bührke 1987 319 275

Mundt, R., Ray, T. P., & Raga, A. C. 1991, A&A 252, 740

Myers, M. R., Beckwith, S. V. W., Herbst, T. M., Robberto, M. 1997, ApJ 489, L173

Ohashi, N., Kawabe, R., Ishiguro, M., Hayashi, M. 1991 AJ 102, 2054

Osterloh, M., Beckwith, S.V.W. 1995, ApJ 439, 299

Padgett, D. L., Brandner, W., et al. 1999, in preparation

Papaloizou, J.C.B., Terquem, C. 1995, MNRAS 274, 987

Raga, A. C. 1995, Rev.Mex.A.Ap, 1, 103

Reipurth, B., Bally, J., Devine, D. 1997, AJ 114, 2708

Richardson, W. H. 1972, J.Opt.Soc.Am., 62, 55

Roddier, C., Roddier, F., Northcott, M. J., Graves, J. E., Jim, K. 1996, ApJ 463, 326

Rodriguez, L. F., Anglada, G., and Raga, A. 1995 Ap.J. 454 L149

Saraceno, P., André, P., Ceccarelli, C., Griffin, M., Molinari, S. 1996, A&A 309, 827

Skinner, S.L, Brown, A., Stewart, R.T. 1993, ApJS 87, 217

Snyder, D.L. 1990, in *The Restoration of HST Images and Spectra*, eds. R.L. White & R.J. Allen, p. 56

Sonnhalter, C., Preibisch, T., Yorke, H. W. 1995, A&A 299, 545

Stapelfeldt, K.R., Burrows, C.J., Krist, J.E. et al. 1995a, ApJ 449, 888

Stapelfeldt, K.R., Burrows, C.J., Koerner, D. et al. 1995b, AAS 187, 113.04

Stapelfeldt, K.R., Burrows, C.J., Krist, J.E. et al. 1997 "Hubble Space Telescope imaging of the disks and jets of Taurus young stellar objects", in *Herbig-Haro Flows and the Birth of Stars* eds. B. Reipurth and C. Bertout, IAU Symposium 182 (Dordrecht: Kluwer), pp. 355–364.

Stapelfeldt, K. R., Krist, J. E., Ménard, F., Bouvier, J., Padgett, D. L., and Burrows, C. J. 1998 ApJ 502 L65

Stapelfeldt, K., Moneti, A. 1999, "The Spectral Energy Distribution of HH 30 as Measured with ISO" in *The Universe As Seen by ISO*, ed. P. Cox, in press

Stapelfeldt, K. R., Padgett, D. L., Brandner, W., et al. 1999, in preparation

Strom, K. M., Strom, S. E., Wenz, M., Wolff, S. C., and Morgan, J. 1986, ApJS 62, 39

Strom, K. M., Strom, S. E., Edwards, S., Cabrit, S., Skrutskie, M. F. 1989, AJ 97, 1451

Strom, K.M, Strom, S.E. 1994, ApJ 424, 237

Strom, S.E. 1994, RMxAA 29, 23

Tamura, M., Gatley, I., Waller, W., Werner, M. W. 1991, ApJ 374, 25

Terebey, S., Vogel, S.N., Myers, P.C. 1989 ApJ 340, 472

Terebey, S., Beichman, C. A., Gautier, T. N., Hester, J. J., Myers, P. C., Vogel, S. N. 1991, in *Astrophysics with Infrared Arrays*, ASP Conf. Series Vol. 14, (San Francisco:ASP), ed. R. Elston, p. 267

Terebey, S., Hancock, T., van Buren, D., Padgett, D. L., Brundage, M. 1999, in preparation

Thompson, R.I., Rieke, M., Schneider, G., Hines, D.C., & Corbin, M.R. 1998, ApJ, 492, L95

Weaver, Wm.B., Jones, G. 1992, ApJS 78, 239

Whitney, B.A., Hartmann, L. 1992, ApJ 395, 529

Whitney, B.A., Hartmann, L. 1993, ApJ 402, 605

Whitney, B.A., Kenyon, S.J., Gomez, M. 1997 ApJ 485, 703

Wood, K., Kenyon, S. J., Whitney, B., and Turnbull, M. 1998, ApJ 497, 404

This preprint was prepared with the AAS LaTeX macros v4.0.

Table 1. Taurus Young Stellar Object Sample.

Target	RA (J2000)	Dec (J2000)	K	Outflow	θ_{of} (°)	MM Continuum Flux (mJy)
IRAS 04016+2610	04 04 42.91	+26 19 02.3	$9\overset{m}{.}33$	optical,mm	180 [1]	180 [2]
CoKu Tau/1	04 18 51.50	+28 20 28.0	$10\overset{m}{.}85$	optical	225 [3]	$\leq$ 12 [4]
Haro 6-5B	04 22 00.69	+26 57 33.3	$9\overset{m}{.}89$	optical	60 [5]	134 [6]
DG Tau B	04 27 02.55	+26 05 30.9	$11\overset{m}{.}52$	optical,mm	122 [7]	310 [8]
IRAS 04248+2612	04 27 57.32	+26 19 19.0	$10\overset{m}{.}65$	optical	172 [9]	99 [10]
IRAS 04302+2247	04 33 16.45	+22 53 20.7	$11\overset{m}{.}07$	optical?,mm?	160 [9]	149 [10]

[1] Hogerheijde et al. 1998

[2] 1.1 mm; Ohashi et al. 1991

[3] Strom et al. 1986

[4] 1.3 mm; Osterloh & Beckwith 1995

[5] Eislöffel & Mundt 1998

[6] 1.3 mm; Dutrey et al. 1996

[7] Mitchell et al. 1997

[8] 1.3 mm; Stapelfeldt et al. 1999

[9] Gomez et al. 1997

[10] 1.1 mm; Moriarty-Schieven et al. 1995

Table 2. Observing log for GO 7418.

Target	Date	F110W	F160W	F187W	F205W
IRAS 04016+2610	Dec 20, 97	768s	768s	512s	256s
CoKu Tau/1	Aug 19, 97	768s	512s	512s	512s
Haro 6-5B	Oct 29, 97	768s	512s	512s	512s
DG Tau B	Dec 21, 97	768s	512s	512s	512s
IRAS 04248+2612	Sep 23, 97	1024s	512s	512s	256s
IRAS 04302+2247	Aug 19, 97	768s	512s	512s	512s

Table 3. Flux values (mJy) (3.″8 aperture).

Target	F110W	F160W	F187W	F205W
DG Tau B	0.59±0.03	4.75±0.10	8.50±0.17	10.7±0.1
IRAS 04016+2610	0.30±0.01	9.58±0.14	21.4±0.3	41.6±0.2
IRAS 04302+2247	0.64±0.02	6.61±0.12	10.2±0.2	11.3±0.1
Haro 6-5B	0.77±0.03	5.79±0.11	10.9±0.2	14.6±0.1
IRAS 04248+2612	6.13±0.10	20.9±0.2	21.3±0.3	20.5±0.2
CoKu Tau/1	6.25±0.09	26.8±0.2	30.2±0.3	29.1±0.2

Table 4. Point Source Fluxes (mJy).

Target	F110W	F160W	F187W	F205W
DG Tau B	0.033±0.006	0.48±0.04	1.25±0.08	2.75±0.07
IRAS 04016+2612	0.021±0.004	1.29±0.04	7.88±0.15	27.4±0.17
IRAS 04302+2247	<0.00056	<0.0023	<0.0048	<0.014
Haro 6-5B	0.39±0.03	2.50±0.08	5.59±0.17	8.64±0.13
IRAS 04248+2612 A [1]	0.85±0.06	3.50±0.13	4.70±0.19	5.80±0.12
IRAS 04248+2612 B [1]	(0.76±0.06)	2.90±0.11	3.70±0.17	4.00±0.10
CoKu Tau/1 A [2]	2.78±0.07	11.1±0.2	13.3±0.24	13.2±0.1
CoKu Tau/1 B [2]	(0.56±0.03)	3.3±0.1	4.7±0.15	5.1±0.1

[1]The eastern component is designated A. The measured binary separation is 0.″160±0.″002 at PA 266° ± 0.5°.

[2]The western component is designated A. The measured binary separation is 0.″240±0.″002 at PA 111° ± 1.4°.

Table 5. Morphological Parameters of Dust Lanes

Target	PA (°)	Major axis (AU)	Minor Axis (AU)	PSF Visibility
DG Tau B	32	600	210	F187W+
IRAS 04016+2610	85	550?	240	F160W+
IRAS 04302+2247	175	1000	340 (110W) - 250 (205W)	None
Haro 6-5B	147	600	150	All filters
IRAS 04248+2612	82	600	220 - 126	All filters
CoKu Tau/1	120	600	50 - 100	F110W+, F160W+

Table 6. Morphological Parameters of Reflection Nebulae

Target	θ_{sa} (°)	Major axis (AU)	Minor Axis (AU)	Opening Angle (°)
DG Tau B	122	550	350	83(e), 45(w)
IRAS 04016+2610	175	1100	850	65(1μm) -160(2μm)
Haro 6-5B	57	560	210	160
IRAS 04302+2247	85	850	400	60
IRAS 04248+2612	170	950	560	60
CoKu Tau/1	210	900	550	92

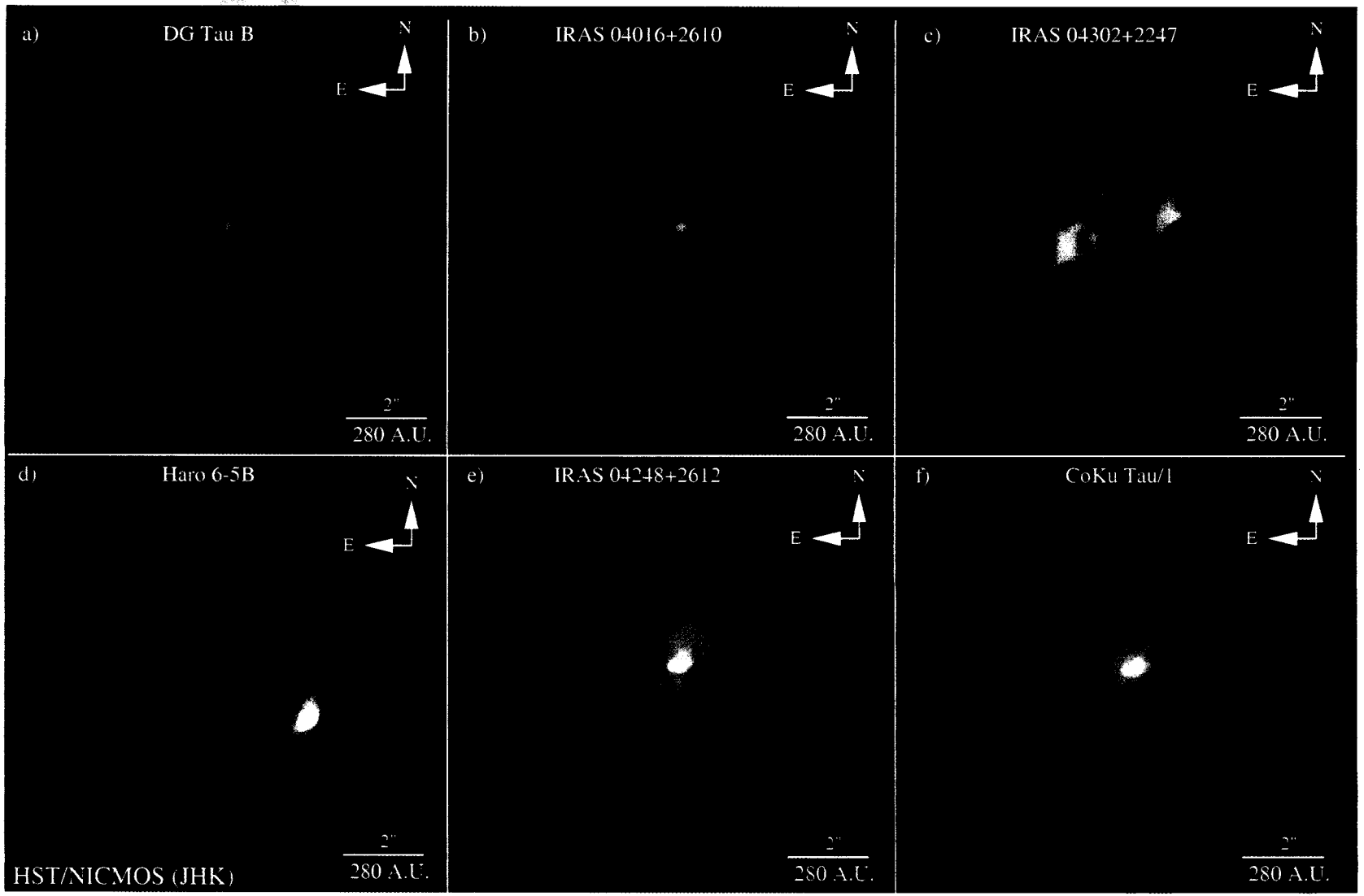

Fig. 1.— HST/NICMOS images of Taurus young stellar objects, arranged in order of decreasing circumstellar mass. These are pseudo-true color composites of NICMOS F110W (1.1 μm), F160W (1.6 μm), and F205W (2.05 μm) broad-band observations. Each image was deconvolved using theoretical point-spread functions, resulting in a factor of 3 reduction in extended PSF features. Note that objects e) and f) are subarcsecond binaries. North is up in all images.

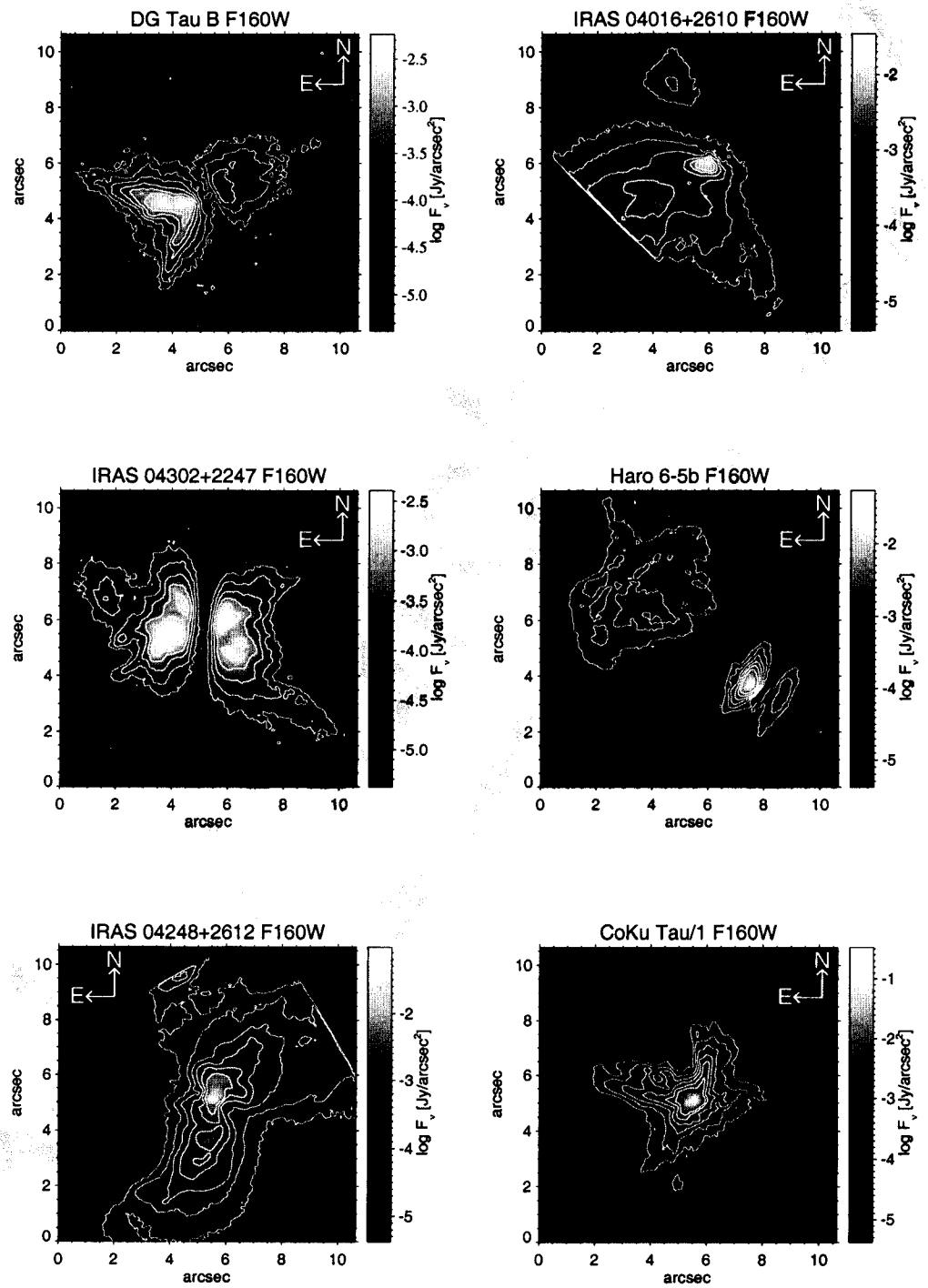

Fig. 2.— Calibrated HST/NICMOS F160W (1.6 μm) broad-band surface photometry for Taurus young stellar objects. As in Figure 1, the images have been deconvolved to a 0.″115 resolution. Contour levels (from left to right, and from top to bottom) start at 0.04 mJy, 0.3 mJy, 0.3 mJy, 0.8 mJy, 2.4 mJy, and 4.7 mJy, respectively, and then double in flux with each subsequent contour level.

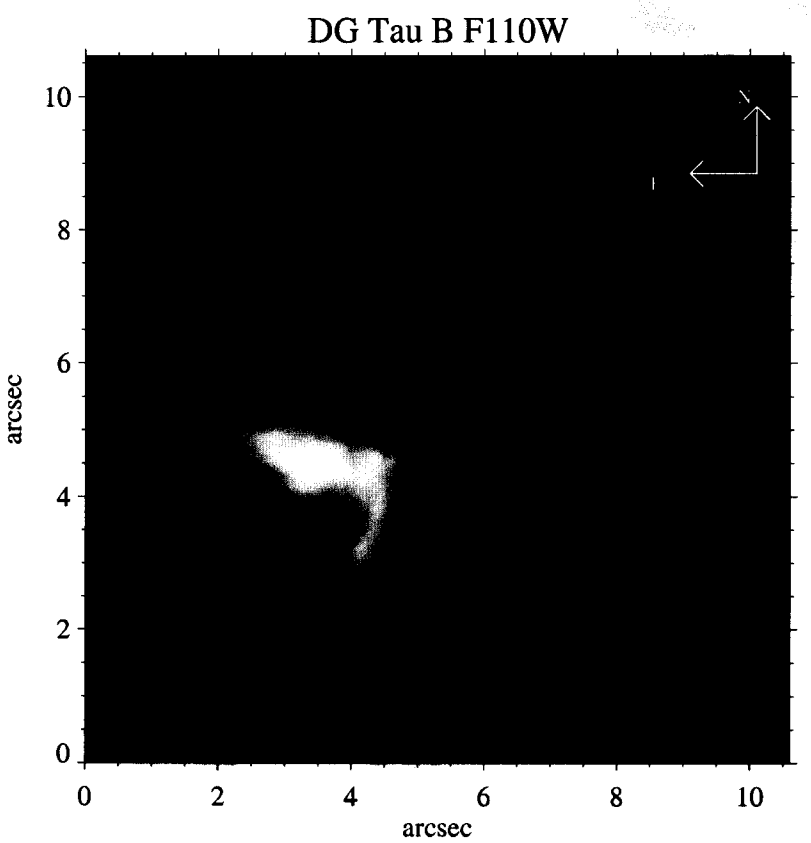

Fig. 3.— HST/NICMOS F110W (1.1 μm broad-band) image of DG Tauri B. Note the linear jet emerging opposite the V-shaped reflection nebula. Emission from jet knots is probably from [Fe II] 1.26 μm.

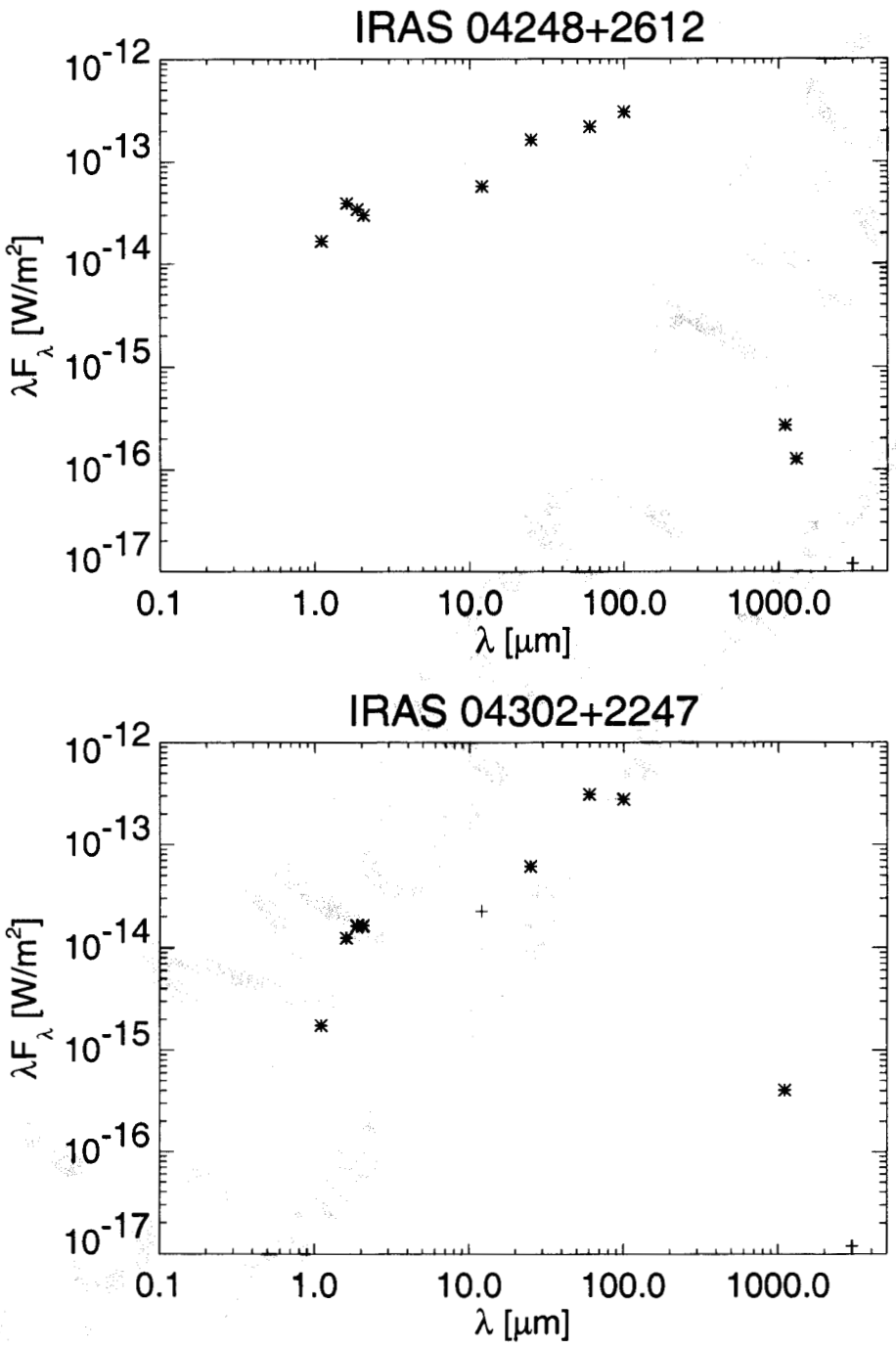

Fig. 4.— Comparison of spectral energy distributions for IRAS 04302+2247 (edge-on Class I YSO) and IRAS 04248+2612 (subarcsecond binary Class I YSO). Asterisks represent measured values, and pluses represent upper limits. Near-infrared points are from the current study, and IRAS fluxes are taken from Beichmann et al. (1992). Millimeter flux densities are from Saraceno et al. (1996), Ohashi et al. (1996), Moriarty-Schieven et al. (1996), and Hogerheijde et al. (1997). Despite the morphological differences between these two objects, the SEDs are very similar. In addition, I04248 has a lower 1 mm flux than I04302, possibly due to clearing of the central portion of the circumbinary disk by the orbital motion of the stars.